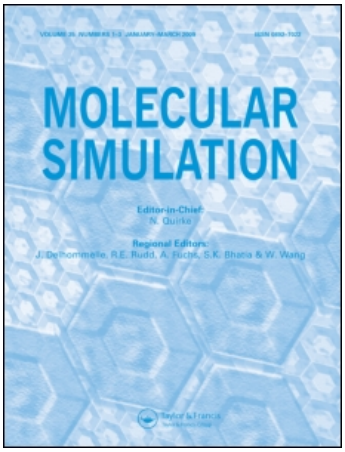

Molecular Simulation
Publication details, including instructions for authors and subscription information:
http://www.informaworld.com/smpp/title~content=t713644482

Statistical mechanics approach to inhomogeneous van der Waals fluids

Shiqi Zhou[a]
[a] Institute of Modern Statistical Mechanics, Hunan University of Technology, Zhuzhou city, P. R. China

To cite this Article Zhou, Shiqi(2006) 'Statistical mechanics approach to inhomogeneous van der Waals fluids', Molecular Simulation, 32: 14, 1165 — 1177
To link to this Article: DOI: 10.1080/08927020601071740
URL: http://dx.doi.org/10.1080/08927020601071740

Molecular Simulation, Vol. 32, No. 14, 15 December 2006, 1165–1177

Taylor & Francis
Taylor & Francis Group

Statistical mechanics approach to inhomogeneous van der Waals fluids

SHIQI ZHOU*

Institute of Modern Statistical Mechanics, Hunan University of Technology, Wenhua Road, Zhuzhou city 412008, P. R. China

(Received June 2006; in final form October 2006)

A general methodology is proposed to formulate density functional approximation (DFA) for inhomogeneous van der Waals fluids. The present methodology needs as input only a hard sphere DFA, second order direct correlation function (DCF) and pressure of coexistence bulk fluid, and therefore can be applicable to both supercitical and subcritical temperature regions. As illustrating example, the present report combines a recently proposed hard sphere "Formally exact truncated non-uniform excess Helmholtz free energy density functional approximation" with the present methodology, and applies the resultant DFA to calculate density profile of the inhomogeneous Lennard-Jones (LJ) fluid in coexistence with a bulk LJ fluid being situated at "dangerous" regions, i.e. the coexistence bulk state is near the critical temperature or the gas-liquid coexistence line. The theoretical predictions are in very good agreement with the recent simulation results, it is concluded that the present DFA is a globally excellent one. A discussion is given why the present methodology can lead to so excellent DFA.

Keywords: Density functional approximation; Potential of mean force; Density functional perturbation approximation; Integral equation theory

1. Introduction

During the last few decades, inhomogeneous fluids had drawn a lot of attention of liquid theoreticians [1]. Inhomogeneous phenomena happen in many fields, such as chemical engineering (adsorption, capillary condensation and wetting transition [2]), molecular biology (molecular interaction [3], i.e. hydrophobic attraction and hydration repulsion), chemistry (solvation free energy [4]) and colloidal science (potential of mean force, tension of surface [1,5]). Theoretical treatment of diverse inhomogeneous phenomena is, in the final analysis, a computation of density profile of the fluid particles near a surface. For example, in a recently proposed universal calculational recipe [5] for the potential of mean force (PMF), the density profile of solvent bath particles around a single solute particle is an indispensable information for calculation of the PMF between two solute particles. A natural choice of theoretical methods for the inhomogeneous phenomena is classical density functional theory (DFT) [1]. The classical DFT approach had witnessed significant progresses during the last decade, most of which happens in the field of hard sphere density functional approximations (DFAs), it is reasonable to conclude that the theoretical formalism for hard sphere DFAs has been highly successful [1]. As for DFAs for non-hard sphere fluids, although a lot of investigations had been conducted by employing the DFAs [6–11], these employed DFAs are not very satisfactory from view point of accuracy. Therefore, the DFAs for non-hard sphere fluids are far from successful.

Several often employed DFT approaches for non-hard sphere fluids are a density functional mean field approximation (DFMFA) [8] and density functional perturbation approximation (DFPA) [8], the other is a partitioned DFA [9–10]. Finally, some researchers also apply directly the hard sphere DFAs to non-hard sphere fluids by substituting the hard sphere second order direct correlation function (DCF) and excess Hemlholtz free energy expressions appearing in the hard sphere DFAs by the corresponding non-hard sphere fluid's counterparts [11]. As for predictive accuracy and applicability of these methods, one can conclude that the DFMFA is very unsatisfactory, the DFPA improves on the DFMFA in some cases, but also becomes unsatisfactory when the coexistence bulk density and temperature are low. One of versions of the partitioned DFA [9] can be very accurate, but the formalism can not work when the temperature

*Email: chixiayzsq@yahoo.com

Molecular Simulation
ISSN 0892-7022 print/ISSN 1029-0435 online © 2006 Taylor & Francis
http://www.tandf.co.uk/journals
DOI: 10.1080/08927020601071740

is below the critical temperature since the formalism needs as input the bulk second order DCF of many state points at the same temperature but different bulk densities, which sometimes enter into an unstable region bounded by a spinodal line. It is well-known that a fluid will separate into low density gas phase and high density liquid phase when the bulk state is in the unstable region where the Ornstein-Zernike (OZ) integral equation theory (IET) has not physical solution. As for the direct application of the hard sphere DFAs to non-hard sphere fluids [11], the resultant formalism will also break down for case of subcritical states due to the same reason as in Ref. [9]. One also notice that previous DFAs [7–11] for non-uniform non-hard sphere fluids had only been tested by simulation data for safe regions of bulk phase diagram, i.e. the regions far away from the critical point, or far away from the gas-liquid coexistence line. Therefore, their performance for regions near critical point or gas-liquid coexistence line is never known.

Aim of the present work is to propose in Section II a methodology into which any hard sphere DFAs can be inserted to formulate DFAs for non-hard sphere fluids under influence of diverse external fields, the resultant DFAs for non-hard sphere fluids will be applicable to both supercritical and subcritical temperature regions. The methodology is combined with a recently proposed hard sphere "Formally exact truncated non-uniform excess Helmholtz free energy density functional approximation (FEHDFA)" due to the present author [12], to formulate DFA for inhomogeneous van der Waals fluids. As illustrating example, the resultant DFA is used to calculate for non-uniform Lennard-Jones (LJ) fluid density profile, and the resultant theoretical results will be compared with the corresponding recently proposed simulation data [6]. Finally, In Section III, we give a detailed analysis about the origin of the excellent performance of the present DFA and some concluding remarks.

2. Methodology for formulating density functional approximation for inhomogeneous van der Waals fluids

In the classical DFT formalism, the density profile equation for a single component fluid reads,

$$\rho(\mathbf{r}) = \rho_b \exp\left\{-\beta\varphi_{\text{ext}}(\mathbf{r}) + C^{(1)}_{\text{ar}}(\mathbf{r};[\rho]) - C^{(1)}_{0\,\text{ar}}(\rho_b)\right\} \tag{1}$$

here $C^{(1)}_{\text{ar}}(\mathbf{r};[\rho])$ and $C^{(1)}_{0\,\text{ar}}(\rho_b)$ are respectively first order DCFs of non-uniform and uniform fluid, $C^{(2)}_{0\,\text{ar}}(r;\rho_b)$ is the second order DCF of the coexistence bulk fluid of density ρ_b, $\varphi_{\text{ext}}(\mathbf{r})$ is an external potential responsible for generation of the non-uniform density distribution $\rho(\mathbf{r})$ of the fluid particles interacting through an arbitrary interparticle potential $u_{\text{ar}}(r)$, $\beta = 1/(kT)$ is the inverse thermal energy with k the Boltzmann's constant and T absolute temperature.

To calculate the $\rho(\mathbf{r})$ by equation (1), a crucial point is to obtain the expression $C^{(1)}_{\text{ar}}(\mathbf{r};[\rho]) - C^{(1)}_{0\,\text{ar}}(\rho_b)$ as a functional of the $\rho(\mathbf{r})$. A formal "Taylor series" expansion of the $C^{(1)}_{\text{ar}}(\mathbf{r};[\rho])$ around the coexistence bulk fluid of density ρ_b can be written down,

$$C^{(1)}_{\text{ar}}(\mathbf{r};[\rho]) - C^{(1)}_{0\,\text{ar}}(\rho_b) = \int d\mathbf{r}_1(\rho(\mathbf{r}_1) - \rho_b)C^{(2)}_{0\,\text{ar}}(|\mathbf{r}-\mathbf{r}_1|;\rho_b) + \sum\nolimits_{\text{ar}}([\rho-\rho_b];\rho_b) \tag{2}$$

here

$$\sum\nolimits_{\text{ar}}([\rho-\rho_b];\rho_b) = \sum_{n=3}^{\infty}\frac{1}{(n-1)!}\int d\mathbf{r}_1\int d\mathbf{r}_2\cdots\int d\mathbf{r}_{n-1} \times\prod_{m=1}^{n-1}[\rho(\mathbf{r}_m)-\rho_b]C^{(n)}_{0\,\text{ar}}(\mathbf{r},\mathbf{r}_1,\ldots,\mathbf{r}_{n-1};\rho_b) \tag{3}$$

the lowest order term $\int d\mathbf{r}_1(\rho(\mathbf{r}_1)-\rho_b)C^{(2)}_{0\,\text{ar}}(|\mathbf{r}-\mathbf{r}_1|;\rho_b)$ in equation (2) is a leading term of the functional perturbation expansion (FPE). Generally speaking, any approximation for the FPE should not damage the leading term! therefore, it is wise for one to keep the leading term intact. In fact, the leading term is also the only term in the expansion which can be calculated by a ready-made theory. Since $C^{(2)}_{0\,\text{ar}}(r;\rho_b)$ can be obtained by solving numerically or analytically the OZ IET, i.e. a combination of OZ IE and a closure relation, as will be discussed later in the paper.

Following the spirit of the partitioned DFT approach [9], we divide the correlation functions into tail part denoted by subscript tail and hard core part denoted by subscript hc, i.e. we have,

$$C^{(2)}_{0\,\text{ar}}(r;\rho_b) = C^{(2)}_{0\,\text{ar}-\text{hc}}(r;\rho_b) + C^{(2)}_{0\,\text{ar}-\text{tail}}(r;\rho_b), \tag{4}$$

$$C^{(1)}_{\text{ar}}(\mathbf{r};[\rho]) = C^{(1)}_{\text{ar}-\text{hc}}(\mathbf{r};[\rho]) + C^{(1)}_{\text{ar}-\text{tail}}(\mathbf{r};[\rho]), \tag{5}$$

and

$$C^{(1)}_{0\,\text{ar}}(\rho_b) = C^{(1)}_{0\,\text{ar}-\text{hc}}(\rho_b) + C^{(1)}_{0\,\text{ar}-\text{tail}}(\rho_b). \tag{6}$$

We have not specified the mathematical detail for dividing these DCFs, in the later part of the paper, one can find that the final outcome does not depend on the detail for the dividing procedure. Since the tail part $C^{(2)}_{0\,\text{ar}-\text{tail}}(r;\rho_b)$ of the second order DCF $C^{(2)}_{0\,\text{ar}}(r;\rho_b)$ is only weakly dependent on the density argument, its treatment by second order functional perturbation expansion approximation (FPEA) is sufficient [9], mathematically one has,

$$C^{(1)}_{\text{ar}-\text{tail}}(\mathbf{r};[\rho]) = C^{(1)}_{0\,\text{ar}-\text{tail}}(\rho_b) + \int d\mathbf{r}_1(\rho(\mathbf{r}_1)-\rho_b)C^{(2)}_{0\,\text{ar}-\text{tail}}(|\mathbf{r}-\mathbf{r}_1|;\rho_b). \tag{7}$$

However, since the hard core part $C^{(2)}_{0\,\text{ar}-\text{hc}}(r;\rho_b)$ is strongly dependent on the density argument ρ_b, the higher order counterpart $C^{(n)}_{0\,\text{ar}-\text{hc}}$ $(n>2)$ of the $C^{(2)}_{0\,\text{ar}-\text{hc}}$ is not a small

quantity, the second order FPEA is certainly not sufficient for treatment of the hard core part, whose theoretical treatment has to incorporate information of higher order terms in the FPE.

Similar to the FPE equation (2), one also has for the hard core part

$$\begin{aligned} & C^{(1)}_{\mathrm{ar-hc}}(\mathbf{r};[\rho\,]) - C^{(1)}_{0\,\mathrm{ar-hc}}(\rho_b) \\ &= \int \mathrm{d}\mathbf{r}_1(\rho(\mathbf{r}_1)-\rho_b)C^{(2)}_{0\,\mathrm{ar-hc}}(|\mathbf{r}-\mathbf{r}_1|;\rho_b) \\ &\quad + \sum\nolimits_{\mathrm{ar-hc}}([\rho-\rho_b];\rho_b) \end{aligned} \tag{8}$$

here

$$\begin{aligned} & \sum\nolimits_{\mathrm{ar-hc}}([\rho-\rho_b];\rho_b) \\ &= \sum_{n=3}^{\infty}\frac{1}{(n-1)!}\int \mathrm{d}\mathbf{r}_1\int \mathrm{d}\mathbf{r}_2\cdots\int \mathrm{d}\mathbf{r}_{n-1} \\ &\quad \prod_{m=1}^{n-1}[\rho(\mathbf{r}_m)-\rho_b]C^{(n)}_{0\,\mathrm{ar-hc}}(\mathbf{r},\mathbf{r}_1,\ldots,\mathbf{r}_{n-1};\rho_b) \end{aligned} \tag{9}$$

Since the expansion coefficients $C^{(n)}_{0\,\mathrm{ar-hc}}(r;\rho_b)$ $(n>2)$ in equation (9) is unknown, one has to approximate the $\sum_{\mathrm{ar-hc}}([\rho-\rho_b];\rho_b)$. The key idea in the present paper is to approximate the $\sum_{\mathrm{ar-hc}}([\rho-\rho_b];\rho_b)$ by the corresponding quantity of the hard sphere fluid with an effective diameter σ_{hs} different from the diameter σ of the fluid particle under consideration. Since properties of the hard sphere fluid is determined by the reduced density $\rho_b\sigma^3_{\mathrm{hs}}$, therefore one also can say that the present key idea is to approximate the $\sum_{\mathrm{ar-hc}}([\rho-\rho_b];\rho_b)$ by the corresponding quantity of the hard sphere fluid with an effective density ρ_{hs} different from the density ρ_b of the fluid particle and diameter σ denoted by $\sum_{\mathrm{hs}}([\rho-\rho_b];\rho_{\mathrm{hs}})$, i.e. we have equality,

$$\sum\nolimits_{\mathrm{ar-hc}}([\rho-\rho_b];\rho_b) = \sum\nolimits_{\mathrm{hs}}([\rho-\rho_b];\rho_{\mathrm{hs}}). \tag{10}$$

Similar to the FPE equation (2), one also has for the hard sphere fluid,

$$\begin{aligned} & C^{(1)}_{\mathrm{hs}}(\mathbf{r};[\rho\,]) - C^{(1)}_{0\,\mathrm{hs}}(\rho_b) \\ &= \int \mathrm{d}\mathbf{r}_1(\rho(\mathbf{r}_1)-\rho_b)C^{(2)}_{0\,\mathrm{hs}}(|\mathbf{r}-\mathbf{r}_1|;\rho_b) \\ &\quad + \sum\nolimits_{\mathrm{hs}}([\rho-\rho_b];\rho_b) \end{aligned} \tag{11}$$

here

$$\begin{aligned} & \sum\nolimits_{\mathrm{hs}}([\rho-\rho_b];\rho_b) \\ &= \sum_{n=3}^{\infty}\frac{1}{(n-1)!}\int \mathrm{d}\mathbf{r}_1\int \mathrm{d}\mathbf{r}_2\cdots\int \mathrm{d}\mathbf{r}_{n-1} \\ &\quad \times\prod_{m=1}^{n-1}[\rho(\mathbf{r}_m)-\rho_b]C^{(n)}_{0\,\mathrm{hs}}(\mathbf{r},\mathbf{r}_1,\ldots,\mathbf{r}_{n-1};\rho_b). \end{aligned} \tag{12}$$

$C^{(2)}_{0\,\mathrm{hs}}(r;\rho_b)$ is the second order DCF of the uniform hard sphere fluid, $C^{(1)}_{\mathrm{hs}}(\mathbf{r};[\rho\,])$ and $C^{(1)}_{0\,\mathrm{hs}}(\rho_b)$ are respectively the non-uniform and uniform first order DCF of the hard sphere fluid, $C^{(n)}_{0\,\mathrm{hs}}$ is the uniform n-order DCF of the hard sphere fluid. Then, we can specify the $\sum_{\mathrm{hs}}([\rho-\rho_b];\rho_{\mathrm{hs}})$ by

$$\begin{aligned} \sum\nolimits_{\mathrm{hs}}([\rho-\rho_b];\rho_{\mathrm{hs}}) &= C^{(1)}_{\mathrm{hs}}(\mathbf{r};[\rho\,],\rho_{\mathrm{hs}}) - C^{(1)}_{0\,\mathrm{hs}}(\rho_{\mathrm{unknown}}) \\ &\quad - \int \mathrm{d}\mathbf{r}_1(\rho(\mathbf{r}_1)-\rho_b)C^{(2)}_{0\,\mathrm{hs}} \\ &\quad \times(|\mathbf{r}-\mathbf{r}_1|;\rho_{\mathrm{hs}}). \end{aligned} \tag{13}$$

It should be pointed out that in equation (13) a density argument ρ_{hs} is added to $C^{(1)}_{\mathrm{hs}}$ and the original argument ρ_b in $C^{(1)}_{0\,\mathrm{hs}}$ is substituted by a unknown density ρ_{unknown} to be in agrement with the substitution of $\sum_{\mathrm{hs}}([\rho-\rho_b];\rho_b)$ by $\sum_{\mathrm{hs}}([\rho-\rho_b];\rho_{\mathrm{hs}})$. Any DFAs for hard sphere fluid, weather they are for the excess Helmholtz free energy [1] or for the non-uniform first order DCF [1,13], all mean an approximation for the $C^{(1)}_{\mathrm{hs}}(\mathbf{r};[\rho\,])$. Then $C^{(1)}_{\mathrm{hs}}(\mathbf{r};[\rho\,],\rho_{\mathrm{hs}})$ can be obtained from $C^{(1)}_{\mathrm{hs}}(\mathbf{r};[\rho\,])$ as will be detailed later in the paper. ρ_{unknown} is specified by ensuring that $\sum_{\mathrm{hs}}([\rho-\rho_b];\rho_{\mathrm{hs}})$ in equation (13) reduces to zero as they should be when the density distribution $\rho(\mathbf{r})$ reduces to ρ_b.

A combination of equations (4)–(8) and (10) then results in

$$\begin{aligned} C^{(1)}_{\mathrm{ar}}(\mathbf{r};[\rho\,]) - C^{(1)}_{0\,\mathrm{ar}}(\rho_b) &= \int \mathrm{d}\mathbf{r}_1(\rho(\mathbf{r}_1)-\rho_b)C^{(2)}_{0\,\mathrm{ar}} \\ &\quad (|\mathbf{r}-\mathbf{r}_1|;\rho_b) + \sum\nolimits_{\mathrm{hs}}([\rho-\rho_b];\rho_{\mathrm{hs}}), \end{aligned} \tag{14}$$

a combination of equations (14) and (13) constitutes the present methodology for approximating the $C^{(1)}_{\mathrm{ar}}(\mathbf{r};[\rho\,]) - C^{(1)}_{0\,\mathrm{ar}}(\rho_b)$ of the inhomogeneous non-hard sphere fluids. Obviously the methodology needs a hard sphere DFA as input.

As an illustrating example, we will employ the recently proposed hard sphere FEHDFA [12] to supply the approximation for $C^{(1)}_{\mathrm{hs}}(\mathbf{r};[\rho\,])$ from which one can derive the $C^{(1)}_{\mathrm{hs}}(\mathbf{r};[\rho\,],\rho_{\mathrm{hs}})$.

The FEHDFA specifies the $C^{(1)}_{\mathrm{hs}}(\mathbf{r};[\rho\,])$ a following form,

$$\begin{aligned} C^{(1)}_{\mathrm{hs}}(\mathbf{r};[\rho\,]) &= C^{(1)}_{0\,\mathrm{hs}}\left(\tilde{\rho}\left(\mathbf{r},\frac{1}{2},\rho_b\right)\right) \\ &\quad + \int C^{(1)'}_{0\,\mathrm{hs}}\left(\tilde{\rho}\left(\mathbf{r}',\frac{1}{2},\rho_b\right)\right) \\ &\quad \times\frac{1}{2}w(|\mathbf{r}-\mathbf{r}'|;\rho_b)[\rho(\mathbf{r}')-\rho_b]\mathrm{d}\mathbf{r}' \end{aligned} \tag{15}$$

$$\begin{aligned} \tilde{\rho}\left(\mathbf{r},\frac{1}{2},\rho_b\right) &= \int \mathrm{d}\mathbf{r}' w(|\mathbf{r}-\mathbf{r}'|;\rho_b) \\ &\quad \times\left[\rho_b+\frac{1}{2}(\rho(\mathbf{r}')-\rho_b)\right] \end{aligned} \tag{16}$$

$$w(|\mathbf{r}-\mathbf{r}'|;\rho_b) = \frac{C^{(2)}_{0\,\mathrm{hs}}(|\mathbf{r}-\mathbf{r}'|;\rho_b)}{C^{(1)'}_{0\,\mathrm{hs}}(\rho_b)} \tag{17}$$

here $C_{0\,\mathrm{hs}}^{(1)'}(\rho_b)$ is the first order density derivative of $C_{0\,\mathrm{hs}}^{(1)}(\rho_b)$, and can be obtained by an exact sum rule: $C_{0\,\mathrm{hs}}^{(1)'}(\rho_b) = \int \mathrm{d}\mathbf{r} C_{0\,\mathrm{hs}}^{(2)}(r;\rho_b)$.

By combining equation (13) with equations (15)–(17), one acquires equation (18)

$$\begin{aligned}
&\sum\nolimits_{\mathrm{hs}}([\rho-\rho_b];\rho_{\mathrm{hs}}) \\
&= C_{0\,\mathrm{hs}}^{(1)}\left(\tilde{\rho}\left(\mathbf{r},\frac{1}{2},\rho_{\mathrm{hs}}\right)\right) - C_{0\,\mathrm{hs}}^{(1)}(\rho_{\mathrm{unknown}}) \\
&\quad + \int C_{0\,\mathrm{hs}}^{(1)'}\left(\tilde{\rho}\left(\mathbf{r}',\frac{1}{2},\rho_{\mathrm{hs}}\right)\right)\frac{1}{2}w(|\mathbf{r}-\mathbf{r}'|;\rho_{\mathrm{hs}}) \qquad (18) \\
&\quad \times[\rho(\mathbf{r}')-\rho_b]\mathrm{d}\mathbf{r}' - \int \mathrm{d}\mathbf{r}_1(\rho(\mathbf{r}_1)-\rho_b)C_{0\,\mathrm{hs}}^{(2)}(|\mathbf{r}-\mathbf{r}_1|;\rho_{\mathrm{hs}})
\end{aligned}$$

here the ρ_{unknown} in equation (18) should be $(\rho_{\mathrm{hs}}+\rho_b)/2$ to ensure that $\sum_{\mathrm{hs}}([\rho-\rho_b];\rho_{\mathrm{hs}})$ denoted by equation (18) reduce sto zero as it should be when the density distribution $\rho(\mathbf{r})$ reduces to ρ_b.

Then, substituting equation (18) into equation (14) leads to the present approximation equation (19) for $C_{\mathrm{ar}}^{(1)}(\mathbf{r};[\rho\,]) - C_{0\,\mathrm{ar}}^{(1)}(\rho_b)$, which is based on the present methodology and the hard sphere FEHDFA [12],

$$\begin{aligned}
C_{\mathrm{ar}}^{(1)}(\mathbf{r};[\rho\,]) - C_{0\,\mathrm{ar}}^{(1)}(\rho_b) &= \int \mathrm{d}\mathbf{r}_1(\rho(\mathbf{r}_1)-\rho_b)C_{0\,\mathrm{ar}}^{(2)} \\
&\quad \times(|\mathbf{r}-\mathbf{r}_1|;\rho_b) \\
&\quad + \sum\nolimits_{\mathrm{hs}}([\rho-\rho_b];\rho_{\mathrm{hs}}) \\
&\quad \text{denoted by Eq.(18)}
\end{aligned} \qquad (19)$$

substituting equation (19) into equation (1) leads to

$$\begin{aligned}
\rho(\mathbf{r}) = \rho_b \exp\Big\{ &-\beta\varphi_{\mathrm{ext}}(\mathbf{r}) + \int \mathrm{d}\mathbf{r}_1(\rho(\mathbf{r}_1)-\rho_b)C_{0\,\mathrm{ar}}^{(2)} \\
&\times(|\mathbf{r}-\mathbf{r}_1|;\rho_b) \quad \sum\nolimits_{\mathrm{hs}}([\rho-\rho_b];\rho_{\mathrm{hs}}) \\
&\text{denoted by equation (18)}\},
\end{aligned} \qquad (20)$$

Equation (20) is the density profile equation of the present DFA, it has to be sovled numerically. In appendix, we will propose a rapid and accurate numerical algorithm for the density profile equation in the classcial DFT approach.

To test the validity and accuracy of the present approximation equation (19), we employ as sample potential a LJ potential $u_{lj}(r)$ truncated and shifted at r_c , the resultant potential $u_{lj}^{ts}(r)$ is given by

$$\begin{aligned}
u_{lj}^{ts}(r) &= u_{lj}(r) - u_{lj}(r_c) \quad r \le r_c \\
&= 0 \qquad\qquad\qquad\quad r \ge r_c
\end{aligned} \qquad (21)$$

$$u_{lj}(r) = 4\varepsilon\left[\left(\frac{r}{\sigma}\right)^{-12} - \left(\frac{r}{\sigma}\right)^{-6}\right] \qquad (22)$$

here, σ is the size parameter or diameter of the LJ particle, ε is the energy parameter and is related with the reduced temperature T^* by $T^* = (kT/\varepsilon)$.

The required second order DCF $C_{0lj}^{(2)}(r;\rho_b)$ of the bulk LJ system in coexistence with the non-uniform LJ fluid under consideration, is obtained by numerically solving the OZ IE equation (23) [14] combined with a closure equation (24).

$$h(r) = C_{0lj}^{(2)}(r;\rho_b) + \rho_b \int \mathrm{d}\mathbf{r}_1 h(\mathbf{r}_1)C_{0lj}^{(2)}(|\mathbf{r}-\mathbf{r}_1|;\rho_b) \qquad (23)$$

$$h(r)+1 = \exp\Big\{-u_{lj}^{ts}(r) + \gamma + B(s)\Big\} \qquad (24)$$

here, indirect correlation function $\gamma = h - C_{0lj}^{(2)}$ with h a total correlation function, $s = \gamma(r) - \beta u_2(r)$ is a so-called renormalization indirect correlation function, the bridge functional B is specified as follows

$$\begin{aligned}
B(s) &= \tfrac{-s^2}{2[1+0.8s]} \quad s \ge 0 \\
&= -0.5s^2 \qquad\quad s < 0
\end{aligned} \qquad (25)$$

bridge functional equation (25) is obtained by substituting a well-known VM bridge functional [15] for $s < 0$ by $-0.5s^2$, and leaving the VM bridge functional for $s \ge 0$ unchanged, the perturbation part $\beta u_2(r)$ of the potential in Ref. [16] is employed in the present paper.

The effective hard sphere density ρ_{hs} in the present methodology is specified by a single hard wall sum rule which declares that the bulk compressibility factor $Z = (\beta P/\rho_b)$ (P is pressure of the coexistence bulk fluid) is equal to the reduced contact density $\rho(0.5\sigma)/\rho_b$ resulting from a single hard wall external potential denoted by equation (26), the P required for this determination is obtained by considering the equality $Z = \rho(0.5\sigma)/\rho_b$, this means that the ρ_{hs} is adjusted to a value ensuring the equality of the contact density predicted by the DFT approach and that obtained by simulation.

Performance of a DFA for non-hard sphere fluids should be judged by comparing its predictions with the corresponding simulation data. A persuasive check adds restrictions on choosing of the simulation data as check standard. Firstly, the external potentials should be of hard wall type, not the type of a steeply repulsive wall with an attractive tail. For latter case, even a mean field approximation for the attractive tail can reproduce satisfactorily the density profile based on the computer simulation, this is why investigation of capillary condensation and wetting phenomena is usually conducted with the weighted density approximation + mean field approximation [7,17]. For the former case, the poor performance of the weighted density approximation + mean field approximation [8] can clearly be seen out. Secondly, the geometrical bodies resulting in the external fields should include not only the single hard wall, but also other cases, such as two hard walls separated by a distance, a large hard sphere, a spherical cavity and a bulk particle. If one only employs the single hard wall

simulation data as performance check, even if the simulation data and theoretical predictions are in very good agreement, there also exists a suspicion that the excellent performance originates from adjusting the $\rho_{\rm hs}$ to ensure the equality of the contact densities predicted by the DFT approach and obtained by simulation. Thirdly, the coexistence bulk fluid state should be near the critical region, i.e. supercritical but very near the critical temperature, or subcritical but near the gas-liquid coexistence curve. In the critical regions, the OZ IET [14] usually can not describe the structure and thermodynamic properties very well, therefore, simulation data for these cases should provide stringent standard for testing a DFA.

Based on the above analysis, the external potentials investigated in the present report are respectively due to a single hard wall as well as two hard walls separated by a distance $H\sigma$, a large hard sphere with radius $R\sigma$, a spherical cavity with a hard wall of radius $R\sigma$, and a bulk particle, the external potentials due to these hard bodies and soft body take the following mathematical forms respectively,

$$\begin{aligned}\varphi_{\rm ext}(z) &= \propto \quad z/\sigma < 0.5 \\ &= 0 \quad 0.5 < z/\sigma\end{aligned} \quad \text{for a single hard wall,} \tag{26}$$

$$\begin{aligned}\varphi_{\rm ext}(z) &= \propto \quad z/\sigma < 0.5 \text{ or } z/\sigma > H - 0.5 \\ &= 0 \quad 0.5 < z/\sigma < H - 0.5\end{aligned} \quad \text{for two hard walls,} \tag{27}$$

$$\begin{aligned}\varphi_{\rm ext}(\mathbf{r}) &= \propto \quad |\mathbf{r}|/\sigma < R \\ &= 0 \quad |\mathbf{r}|/\sigma > R\end{aligned} \quad \text{for a large hard sphere,} \tag{28}$$

$$\begin{aligned}\varphi_{\rm ext}(\mathbf{r}) &= 0 \quad |\mathbf{r}|/\sigma < R \\ &= \infty \quad |\mathbf{r}|/\sigma > R\end{aligned} \quad \text{for a hard spherical cavity,} \tag{29}$$

$$\varphi_{\rm ext}(\mathbf{r}) = u_{lj}^{ts}(r) \text{ for a bulk particle.} \tag{30}$$

For the last case of equation (30), the reduced density profile $\rho(\mathbf{r})/\rho_b$ is exactly the bulk fluid radial distribution function (RDF) $g(\mathbf{r})$.

Now we will employ the recently proposed simulation data of coexistence bulk LJ fluid near critical region to test the present DFA. Ref. [6] supplied enough simulation data for LJ fluid with $r_c = 100\sigma$ subjected to diverse external potentials denoted by equations (26)–(30). Theoretical predictions for the density profiles of LJ fluid subjected to diverse external fields and the corresponding simulation data for two sets of bulk density and reduced temperature are displayed in figures 1–9. In turn, the figures show the density profiles of the LJ fluid: (i) at a single hard wall (figures 1 and 2), (ii) in the hard planar gap of width $H = 3\sigma$ (figures 3 and 4), (iii) in a hard spherical cavity of effective radius $R = 3.5\sigma$ (figures 5 and 6), (iv) a large hard sphere particle of varying radius (figures 7 and 8), and (v) a bulk LJ particle (figure 9). The corresponding values for the effective hard sphere reduced density $\rho_{\rm hs}\sigma^3$ are also

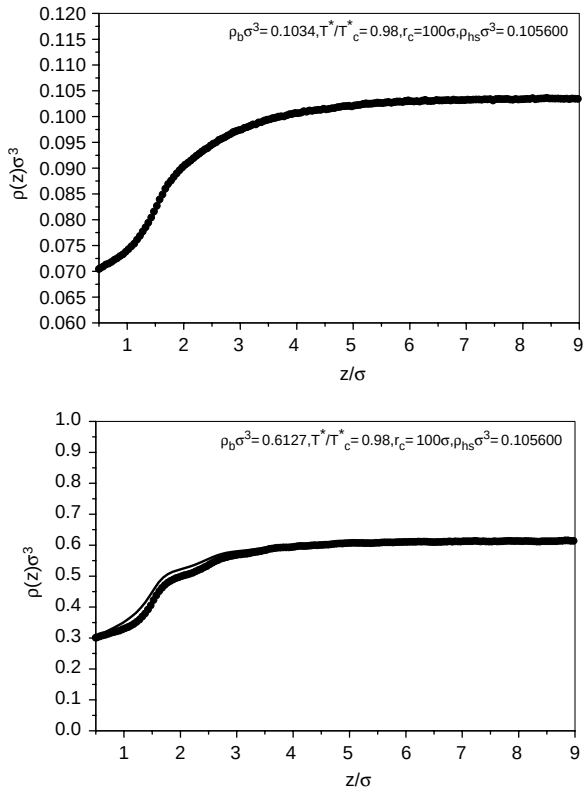

Figure 1. Density profile for a LJ fluid truncated and shifted at $r_c^* = r_c/\sigma = 100$ near a hard wall. The symbols are for the MC data [6], the lines are for the present theoretical predictions.

presented. For the sake of clarity, some of figures are subdivided into two parts, which successively illustrate the results of increasing coexistence bulk densities at constant values of reduced temperature T^*. When the inhomogeneous structure of the fluid stems from the presence of a single wall, flat density profiles $\rho(z) = \rho_b$ are restored at sufficient distances from the wall, irrespective of the specific values of the coexistence bulk fluid parameters.

A comparison of the theoretical predictions and the simulation data for the local structure of the LJ fluid in

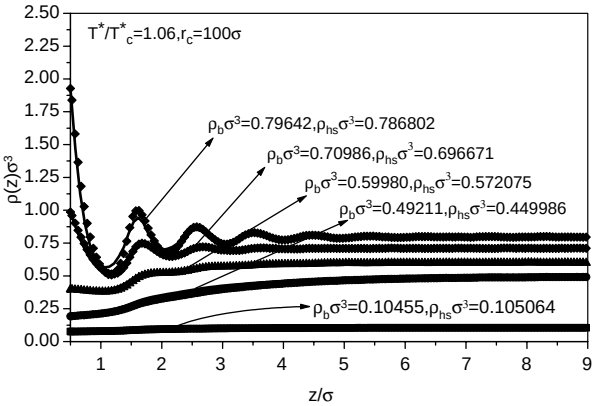

Figure 2. Same as in figure 1 but the temperature T^* and coexistence bulk densities.

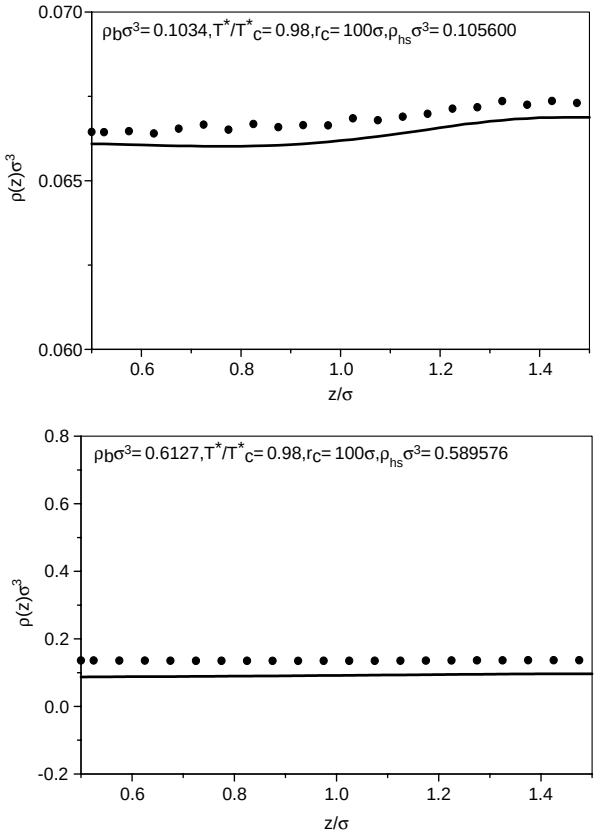

Figure 3. Same as in figure 1 but for an external field due to two hard walls with $H = 3$.

various inhomogeneous systems indicates a very good accuracy of the present DFT approach. Especially, the actual performance is very little dependent on the external potentials responsible for the generation of the density profiles, this observation lends strong support to the validity of the present DFA. If the excellent agreement between theory and simulation for case of the single hard wall is not due to the inherent appropriateness of the DFA, but due to ajdusting the $\rho_{\rm hs}\sigma^3$ to arrive at an equality between the contact density from two routes, then the excellent performance at most is possible for the single hard wall case, will not persist for other external potentials. Considering that the testing simulation data are all from the "dangerous" regions of the bulk phase diagram, one can confidently conclude that the present DFA is surely inherently structured soundly, and is a globally excellent DFA for the inhomogeneous LJ fluid. A comparison between figure 3 in the present paper and figure 3 in Ref. [6] also indicates that the present approach is more accurate than the recently proposed third order + second order perturbation DFT approach.

We have also performed computations at several bulk densities for reduced temperature $T^* = 1.35$, which is supercritical and far away from the critical temperature, and compared the DFT calculational results with the Monte Carlo simulational results of Balabanic *et al.* [18]. The value of the cutoff distance r_c used in the MC simulations varied with bulk densities, but these values are estimated to be close to 4.0σ. We find (figure 10) that the present DFT formalism achieves higher prediction accuracy than previous DFPT [7,8] and DFMFT [7,8] at the low, middle and high densities for case of the supercritical temperature $T^* = 1.35$. The present prediction accuracy is also higher than a recently proposed DFT approaches [10]. The observation that in subfigure a, the dotted line is in more satisfactory agreement with simulation result than the solid line indicates that an accurate EOS can help improve the performance of the present DFT approach.

There do not exist bulk coexistence pressure data for the state points in figure 10, therefore it is necessary to give a discussion about the bulk pressure employed to determine the $\rho_{\rm hs}\sigma^3$ in figure 10. An accurate EOS [19] is available for bulk LJ fluid, which is obtained by fitting the computer simulation data, however the EOS is for LJ potential without truncation (i.e. $r_c = \propto$). To calculate the bulk pressure for truncated and shifted LJ potential with the EOS, one has to correct the EOS with thermodynamic perturbation theory as done in the present paper.

$$Z(\rho_b, T^*, r_c) = \frac{\beta P(\rho_b, T^*, r_c)}{\rho_b} = Z^{LJ}(\rho_b, T^*) + \rho_b \frac{\partial \beta\phi}{\partial \hat{\rho}}\bigg|_{\hat{\rho}=\rho_b} \tag{31}$$

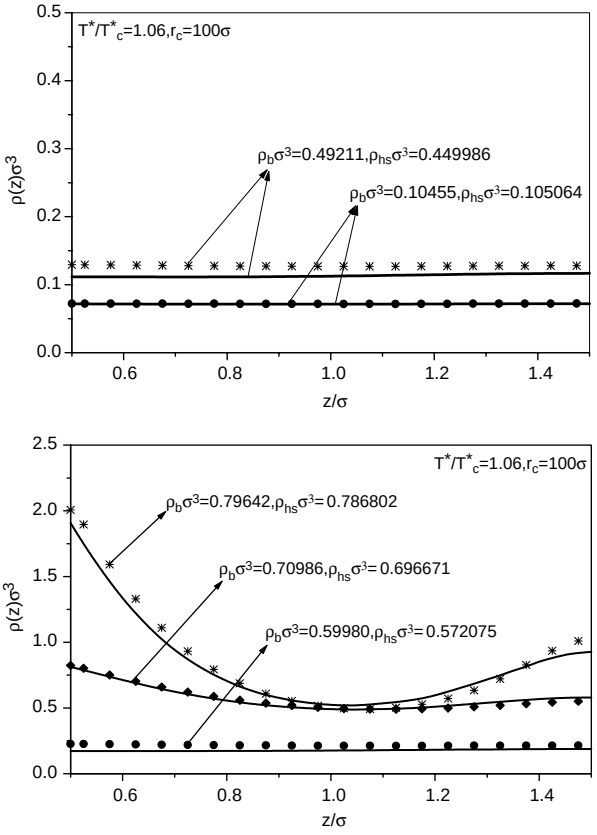

Figure 4. Same as in figure 2 but for an external field due to two hard walls with $H = 3$.

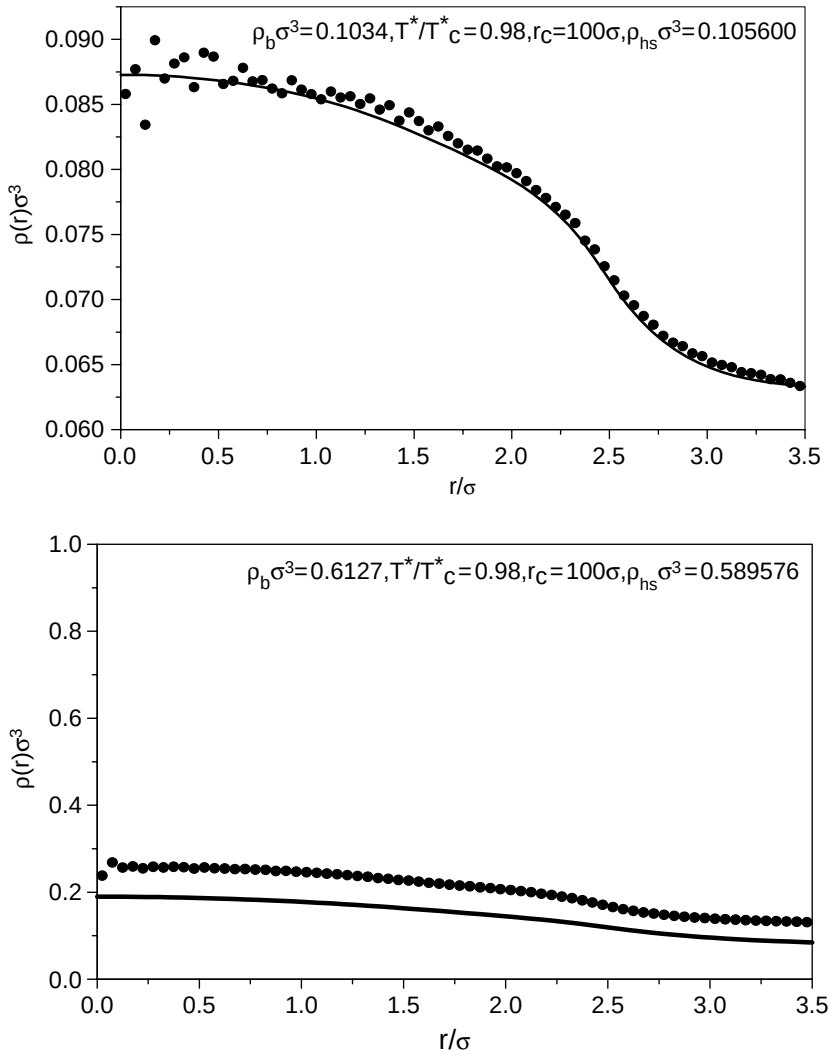

Figure 5. Same as in figure 1 but for an external field due to a hard spherical cavity with $R = 3.5$.

$Z^{LJ}(\rho_b, T^*)$ is the compressibility factor of the LJ fluid without truncation, which can be obtained from the EOS [19]. The thermodynamic correction for the reduced excess Helmholtz free energy per particle is:

$$\beta\phi(\hat{\rho}, T^*, r_c) = 2\pi\hat{\rho}\int g(r, \hat{\rho}d(\hat{\rho}, T^*)^3)\beta u_{ts}(r)r^2 \mathrm{d}r \quad (32)$$

here

$$\begin{aligned} \beta u_{ts}(r) &= -\beta u(r_c) \quad r < r_c \\ &\quad -\beta u(r) \quad r > r_c \end{aligned} \quad (33)$$

$g(r, \hat{\rho}\mathrm{d}(\hat{\rho}, T^*)^3)$ is the RDF of the hard sphere fluid of reduced bulk density $\hat{\rho}\mathrm{d}(\hat{\rho}, T^*)^3$ and equivalent hard sphere diameter $\mathrm{d}(\hat{\rho}, T^*)$, and is given by the Verlet-Weis prescription [20]. Regarding the specification of $\mathrm{d}(\hat{\rho}, T^*)$, we employ a simple interation procedure also due to Verlet and Weis [20].

3. Discussion and concluding remarks

The present paper proposes a methodology into which any hard sphere DFAs can be inserted to formulate a DFA for inhomogeneous van der Waals fluids. As illustrating example, the present paper combines the methodology with the hard sphere FEHDFA [12] to investigate the solid-liquid interface structure behavior of the LJ fluid, extensive DFT model calculation and comparison with simulation data have shown the excellent predictive performance of the resultant DFA. Considering that the simulation data correspond to coexistence bulk fluid states situated at "dangerous" regions in the bulk diagram, it is fair to say that the present DFA, based on the combination of the present methodology and the hard sphere FEHDFA, is a globally excellent approximation for the non-uniform LJ fluid. Although the DFA in Ref. [10] also seems satisfactory for some bulk states, its accuracy is strongly dependent on a choosing of an effective hard sphere diameter. However, an empirical formulae relating the

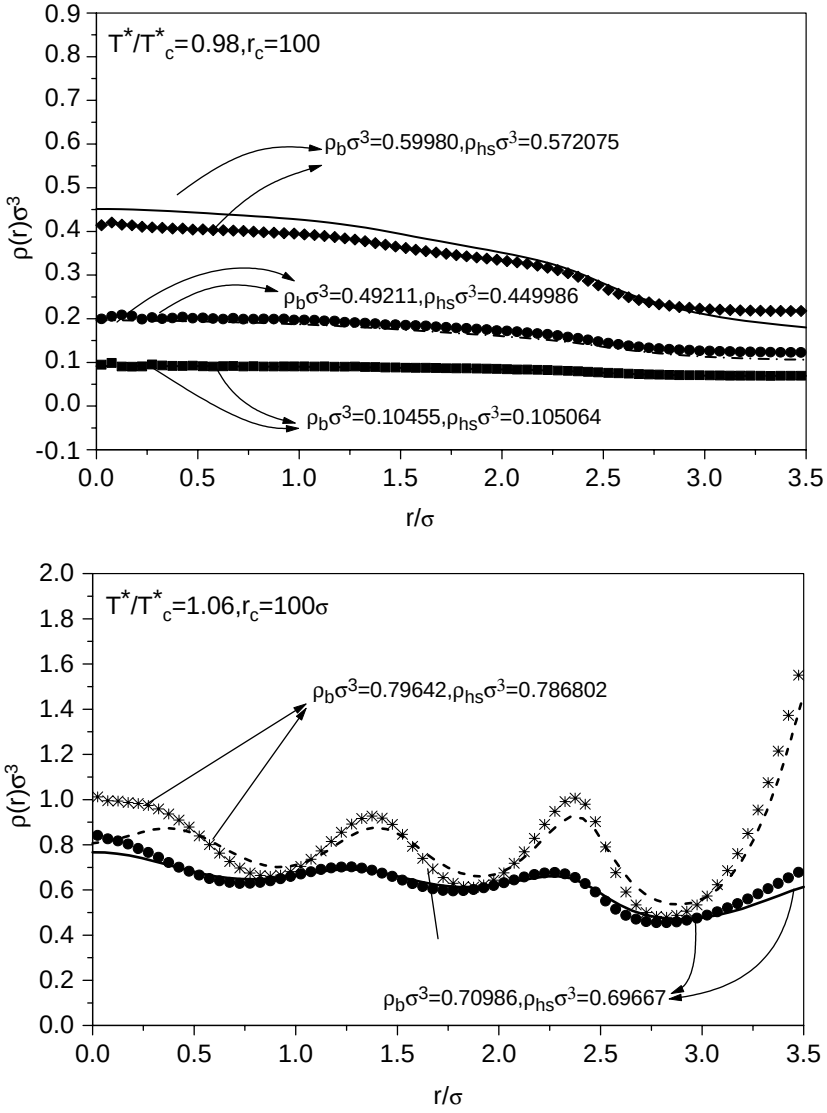

Figure 6. Same as in figure 2 but for an external field due to a hard spherical cavity with $R = 3.5$.

effective hard sphere diameter and the size parameter σ employed in Ref. [10] maybe not sufficient to ensure the global performance of the DFA in Ref. [10].

It is worth to giving a detailed analysis why such excellent DFA can be drawn forth from the present methodology even if the latter is combined with the hard sphere FEHDFA whose performance for non-uniform hard sphere fluid in fact is not very satisfactory. Firstly, unlike the Ref. [10], the present paper provides a mechanism to specify the $\rho_{\rm hs}\sigma^3$, it is equal to say that the present paper provides a mechanism to specify the effective hard sphere diameter as discussed in the text. Although the Ref. [10] also can be devoid of the empirical formulae by specifying the effective hard sphere diameter with the single hard wall sum rule as done in the present paper, the present $\rho_{\rm hs}\sigma^3$ appears not only as the density argument of the hard sphere correlation functions, but also in $\tilde{\rho}(\mathbf{r}(1/2), \rho_{\rm hs})$, the lowest layer of the theoretical structure. Thus, a changing of $\rho_{\rm hs}\sigma^3$ will lead to a whole displacement of the density field ($\tilde{\rho}(\mathbf{r}, (1/2), \rho_{\rm hs})$ appears as the argument of $C^{(1)'}_{0\,\rm hs}$ which is parallel with the density field $\rho(\mathbf{r}) - \rho_b$ in equation (18). The present relationship between the $\rho_{\rm hs}\sigma^3$ and the density profile $\rho(r)$ is strongly non-linear, therefore is superior to the practice in Ref. [10] where the effective hard sphere diameter only appears as the argument of the hard sphere correlation function. However, this point is not the main reason why the present DFA performs so well. The main reason for the success of the present methodology, or the basic difference of the present methodology from previous one [7,8], is that the previous methodology [7,8] consists of combining a hard sphere DFA for an effective hard sphere fluid with the effective hard sphere diameter depending on the potential parameter (such as temperature) and bulk density, with a mean field approximation for tail part of the potential, therefore the previous methodology completely damages the lowest order term by distorting the bulk second order DCF. As is discussed in the text, from the view of the FPE,

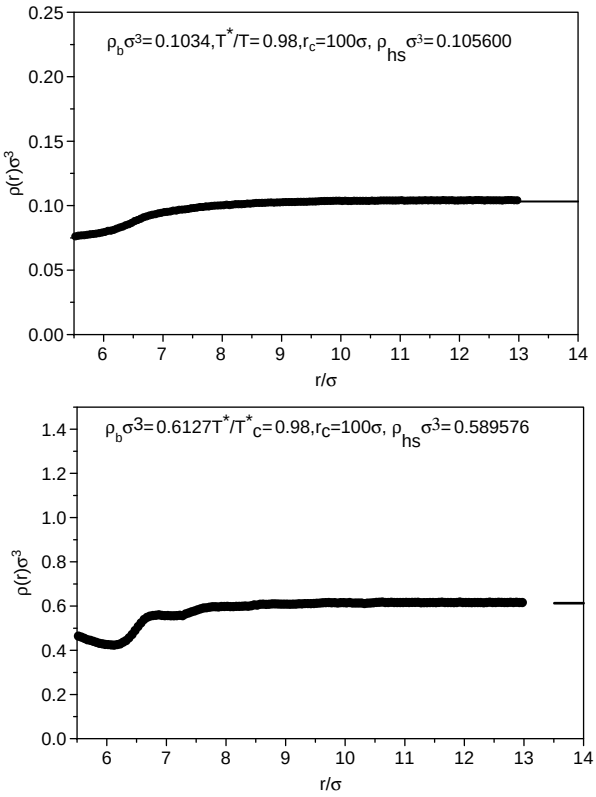

Figure 7. Same as in figure 1 but for an external field due to a large hard sphere particle with $R = 5.5$.

the lowest order term is the leading term which contains much information of the density functional, a necessary condition for a DFA to be excellent is to correctly treat the leading term. The previous methodology [7,8] also contains a term formally similar to the leading term, but the bulk second order DCF there is a sum of bulk hard sphere second order DCF of an effective hard sphere fluid and the minus tail part of the reduced potential, very different from the very accurate bulk second order DCF by solving numerically the OZ ITE. Therefore, the previous methodology does not perform so well. While the present methodology keeps the leading term of the FPE intact, the bulk second order DCF is based on very accurate numerical solution of the OZ IET. Therefore, from the view of the leading term of the FPE, the present methodology is superior to the previous methodology [7,8]. As for the treatment on the higher order terms of the FPE, the both methodologies are the same. They all employ the hard sphere DFA to treat the higher order terms of the FPE for the effective hard sphere fluid. How to explain the better performance of the DFA in Ref. [10] than that in Ref. [7,8]? The DFA in Ref. [10] consists of combining the hard sphere fundamental measure functional [21,1] to treat the effective hard sphere fluid and second order FPEA for the tail part, in treating the tail part, as done in Ref. [9] and the present paper, Ref. [10] employs the tail part of an analytical bulk second order DCF. Therefore, Ref. [10]'s treatment on the tail part is more accurate than that in Ref. [7,8]. How to explain the better performance of the present DFA than that in Ref. [10]? The present methodology keeps the leading term intact, but the DFA in Ref. [10] only keeps the tail part of the leading term intact. Therefore, the present DFA is superior to those in Refs. [7,8,10].

Unlike the DFA in Ref. [9], the present DFA only needs as input the second order DCF of the coexistence bulk fluid, it is therefore applicable to both supercritical and subcritical regions as shown in the paper. Acceptance of the numerical bulk second order DCF as input also essures the convenient extension of the present methodology to other model potentials or even the solvent-mediated potentials [22] which, depending on the solvent bath peoperties, is of diverse mathematical forms whose analytical bulk second order DCF is therefore unavailable. We will report further investigation based on the present methodology for other inhomogeneous van der Waals fluids or even the solvent-mediated potentials [22].

Acknowledgements

The author would like to thank the reviewers for helpful comments. This project is supported by the National Natural Science Foundation of China (20673150).

Appendix

Calculation of self-consistent solution is a ubiquitous problem in the fields of computational physics and chemistry. Classical DFT approach has now evolved into a powerful theoretical tool for investigation on structure and thermodynamic properties of inhomogeneous fluids. However, rapid and accurate algorithm is not yet reported for numerical solution of density profle equation in the classical DFT approach, this hinders the widespread application of the classical DFT approach as a routine tool.

A common strategy to obtain self-consistent solution is by iterative calculations. Traditional iterative procedure is a Picard iteration method [23] which however results in poor convergence behavior: either slow convergence even with a good initial guess or divergence at all. The divergence of the Picard method [23] can be cured by Broyles' mixing procedure [24], if a good initial estimate is available, but the convergence is still generally slow especially when the bulk density is high. In the present paper, we apply an inverse Broyden method to the iteration solution of the density profile equation denoted by equation (20) in combination with equation (18).

The input quantity $C^{(2)}_{0\,\mathrm{ar}}(r;\rho_b)$ is obtained by solving numerically the OZ IET equations (23)–(25) with help of an algorithm due to Labik *et al.* [25], $C^{(1)}_{0\,\mathrm{hs}}(\rho_b)$ and $C^{(2)}_{0\,\mathrm{hs}}(r;\rho_b)$ can be analytically obtained by a Percus-Yevick (PY) approximation [26].

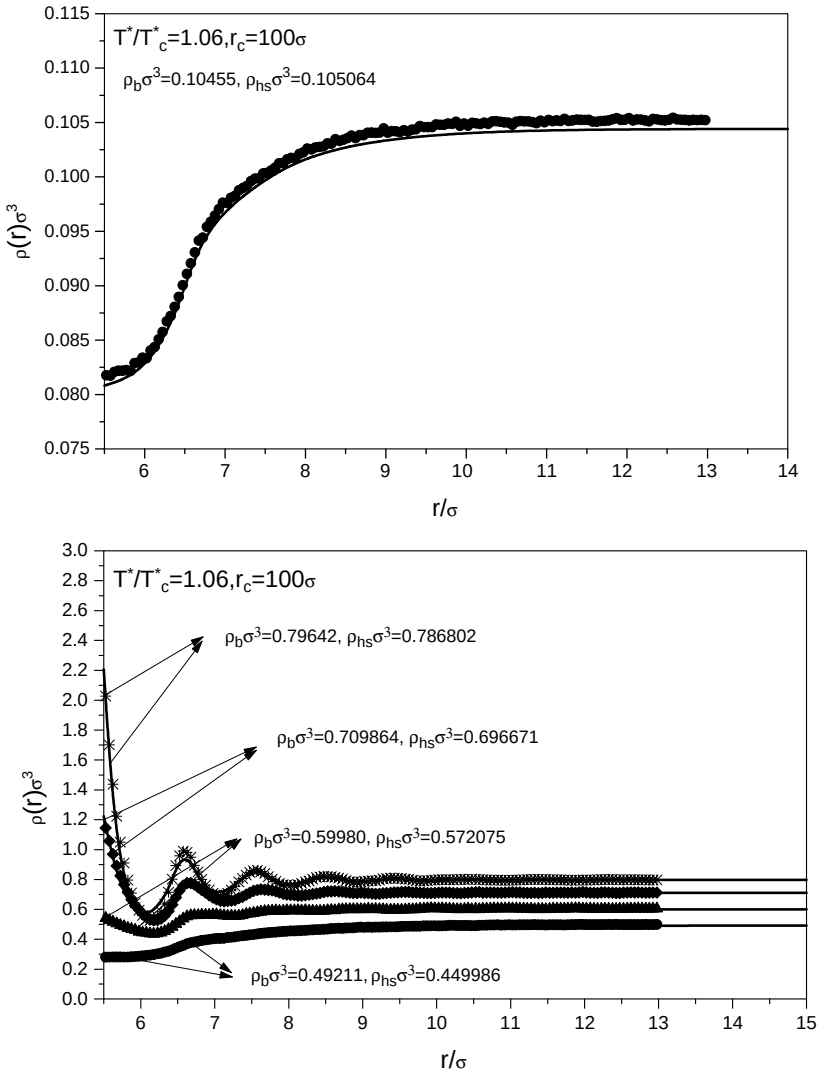

Figure 8. Same as in figure 2 but for an external field due to a large hard sphere particle with $R = 5.5$.

The algorithm for numerical solution of density profile equation (20) is described as follows, as an example, we employ the external potential denoted by equation (28) to illustrate the algorithm. We solve the density profile equation on a grid of equal distance Δr from $r = R\sigma$ to $r = R\sigma + 14\sigma$,

$$\rho^i(R\sigma + (i-1)\Delta r), \quad i = 1, 2, \ldots N \tag{A1}$$

$$\begin{aligned} \rho(\mathbf{r}) &= 0, \qquad r < R\sigma \\ &\rho_b, \qquad r > R\sigma + 14\sigma \end{aligned} \tag{A2}$$

the numerical value of $\rho(r)$ on space between grid points can be obtained by interpolation. The 3D integral $\int d\mathbf{r}_1(\rho(\mathbf{r}_1) - \rho_b)C^{(2)}_{0\,\mathrm{ar}}(|\mathbf{r} - \mathbf{r}_1|; \rho_b)$ in equation (20) can be reduced to a 2D integral

$$2\pi\int_0^{r'} dr'' \int_0^{\pi} d\theta r''^2 \sin\theta C^{(2)}_{0\,\mathrm{ar}}(r''; \rho_b) \times \left[\rho\left(\sqrt{r''^2 + r^2 + 2rr''\cos(\theta)}\right) - \rho_b\right]$$

the integral on radial distance r'' is done by simple Trapezoidal rule [27], while the angle integral is done by Gaussian method [27]. For LJ fluid, $r' = 7\sigma$ is sufficient. It should be noted that the expression

$$\rho\left(\sqrt{r''^2 + r^2 + 2rr''\cos(\theta)}\right)$$

in the integrand is non-continuous as a function of θ, therefore, the angle integral should be seperated into several regions in which the function is continuous. The integral $\int d\mathbf{r}_1(\rho(\mathbf{r}_1) - \rho_b)C^{(2)}_{0\,\mathrm{hs}}(|\mathbf{r} - \mathbf{r}_1|; \rho_{\mathrm{hs}})$ and

$$\int C^{(1)'}_{0\,\mathrm{hs}}\left(\tilde{\rho}\left(\mathbf{r}', \frac{1}{2}, \rho_{\mathrm{hs}}\right)\right)\frac{1}{2}w(|\mathbf{r} - \mathbf{r}'|; \rho_{\mathrm{hs}})[\rho(\mathbf{r}') - \rho_b]\, d\mathbf{r}'$$

in equation (18) can be done similarly. However, to integrate the latter, one has to firstly calculate the $\tilde{\rho}(r, (1/2), \rho_{\mathrm{hs}})$. Similar to the treatment of the density profile $\rho(r)$, one also can only calculate the $\tilde{\rho}(r, (1/2), \rho_{\mathrm{hs}})$ on a grid of equal distance Δr from $r = \max(R\sigma - \sigma, 0)$

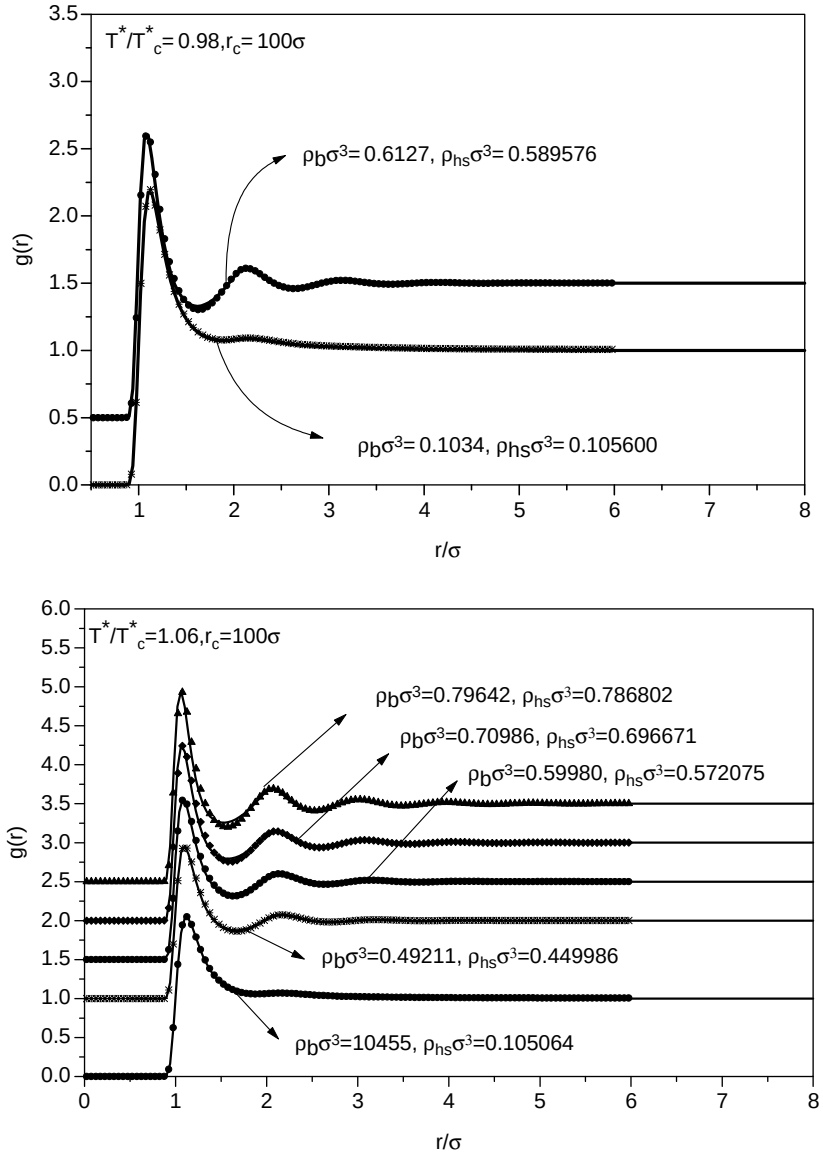

Figure 9. The RDF for several different states of the coexistence bulk LJ fluid truncated and shifted at $r_c^* = r_c/\sigma = 100$. Subfigure a is for subcritical coexistence bulk fluids, the above line and symbol should be moved downward 0.5. Subfigure b is for supercritical coexistence bulk fluids, the above lines and symbols from top to bottom should be moved downward 2.5, 2, 1.5, 1, respectively. Lines are for present theoretical predictions, while symbols are for the corresponding simulation data [6].

to $r = R\sigma + 15\sigma$, i.e.

$$\tilde{\rho}^j(\max(R\sigma - \sigma, 0) + (j-1)\Delta r), \quad j = 1, 2, \ldots N'$$

the numerical value of $\tilde{\rho}(r, (1/2), \rho_{\mathrm{hs}})$ on space between grid points also can be obtained by interpolation.

Based on the above analysis, one can write the density profile equation (20) into a non-linear equation system with N un-knowns

$$\begin{aligned} \rho^i &= f(R\sigma + (i-1)\Delta r; \lfloor \rho^1, \rho^2, \ldots, \rho^N \rfloor) \\ i &= 1, 2, \ldots, N \end{aligned} \tag{A3}$$

here, f denotes the functional relationship of equation (20).

Algorithm formulae of the inverse Broyden method [28] can be summarized as follows,

$$\begin{aligned} \mathbf{x}^{k+1} &= \mathbf{x}^k - \mathbf{H}_k \mathbf{F}(\mathbf{x}^k) \\ \mathbf{H}_{k+1} &= \mathbf{H}_k + \alpha(\mathbf{s}^k - \mathbf{H}_k \mathbf{y}^k) \frac{(\mathbf{s}^k - \mathbf{H}_k \mathbf{y}^k)^T}{(\mathbf{s}^k - \mathbf{H}_k \mathbf{y}^k)^T \mathbf{y}^k} \\ k &= 0, 1, \ldots \end{aligned} \tag{A4}$$

where k denotes the kth iteration, $\mathbf{s}^k = \mathbf{x}^{k+1} - \mathbf{x}^k$, $\mathbf{y}^k = \mathbf{F}(\mathbf{x}^{k+1}) - \mathbf{F}(\mathbf{x}^k)$, $\mathbf{H}$ is $N \times N$ iterative matrix, $\mathbf{x}$ is

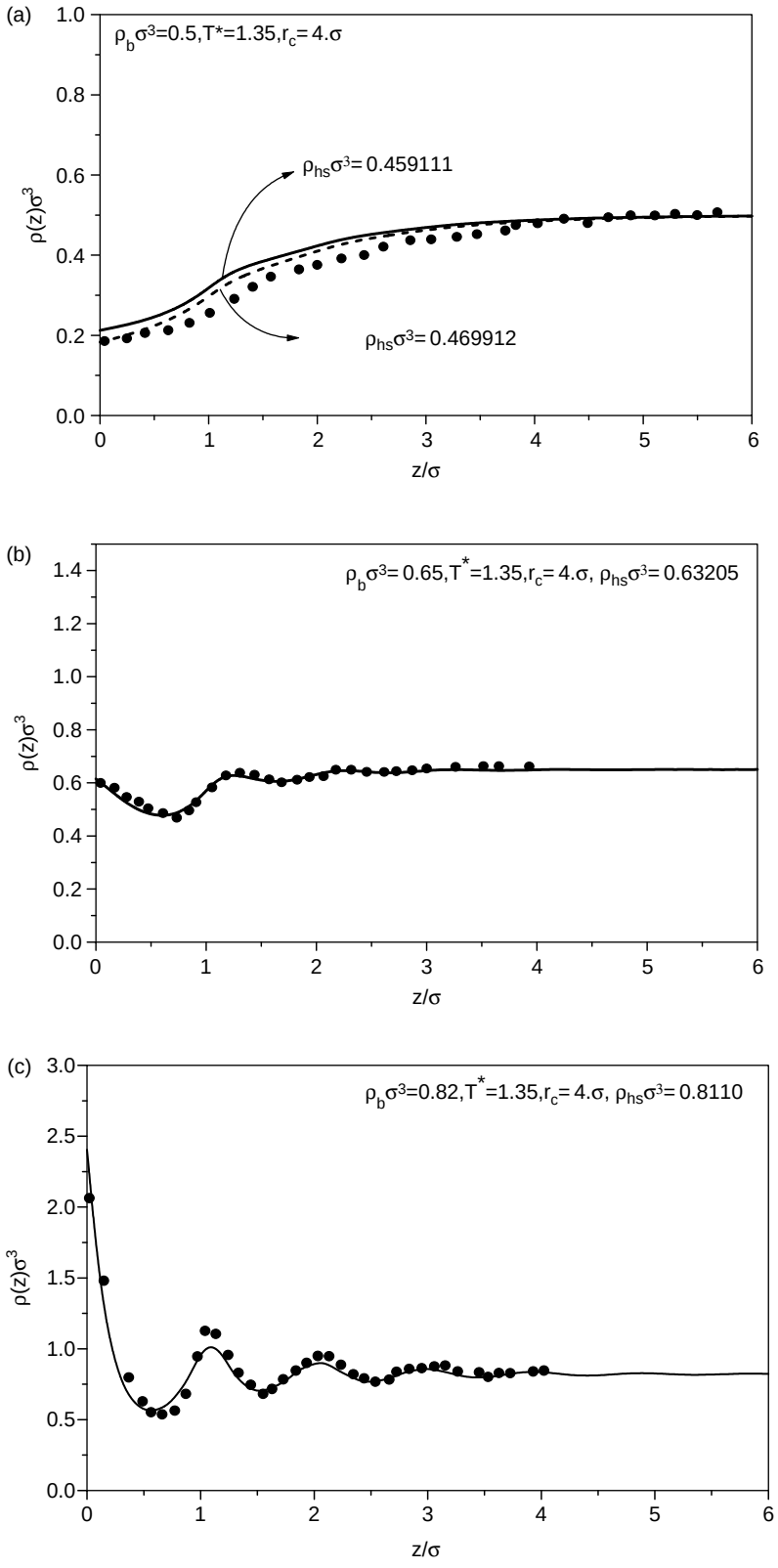

Figure 10. Density distribution profile for a LJ (truncated and shifted at $r_c^* = r_c/\sigma = 4$) fluid in contact with a single hard wall at the reduced temperature $T^* = 1.35$ and the coexistence bulk density $\rho_b\sigma^3 = 0.5$(a), 0.65 (b), 0.82 (c). The symbols are for the MC data [18], the lines are for the present theoretical predictions. In subfigure a, the dotted line is based on an value of $\rho_{hs}\sigma^3$ from the contact density, while the solid line from the present corrected EOS, in subfigure b and c, the solid lines are based on an value of$\rho_{hs}\sigma^3$ from the present corrected EOS.

the $N \times 1$ matrix given by

$$\mathbf{x} = \begin{bmatrix} \rho^1 \\ \rho^2 \\ . \\ . \\ . \\ \rho^N \end{bmatrix} \tag{A5}$$

$\mathbf{F}$ is the $N \times 1$ matrix given by

$$\mathbf{F}(\mathbf{x}) = \begin{bmatrix} \rho^1 - f\left(R\sigma + (1-1)\Delta r; \left[\rho^1, \rho^2, \ldots \rho^N\right]\right) \\ \rho^2 - f\left(R\sigma + (2-1)\Delta r; \left[\rho^1, \rho^2, \ldots \rho^N\right]\right) \\ . \\ . \\ . \\ \rho^N - f\left(R\sigma + (N-1)\Delta r; \left[\rho^1, \rho^2, \ldots \rho^N\right]\right) \end{bmatrix} \tag{A6}$$

When $\mathrm{Re}\, sidual = \mathbf{F}^T\left(\mathbf{x}^k\right)\mathbf{F}\left(\mathbf{x}^k\right) \leq \varepsilon$($\varepsilon$ is absolute error, usually 10^{-5} or 10^{-9}), $\mathbf{x}^k$ is the true solution. To initiate iteration process of the inverse Broyden method, one has to input the $\mathbf{x}^0$ and $\mathbf{H}_0$. In the original inverse Broyden method, coefficient α is equal to 1, the present practice indicates that lowering the α to a lower value, for example 0.8, can prevent the iteration process from diverging.

Throughout the presented calculations, $\Delta r = 0.04\sigma$, therefore $N = 14\sigma/\Delta r + 1 = 351$, $N' = 16\sigma/\Delta r + 1 = 401$.

For case of low bulk density $\rho_b\sigma^3$, for example $\rho_b\sigma^3 \leq 0.45$, the initial values are set to be $\mathbf{x}^{0^T} = [\rho_b, \rho_b, \ldots \rho_b]$ and $\mathbf{H}_0$ =unit matrix, α can be set to be 1, after 6–7 iterations, the true solution with $\varepsilon = 10^{-9}$ can be found. When $\rho_b\sigma^3 > 0.45$, the iteration process with $\mathbf{x}^{0^T} = [\rho_b, \rho_b, \ldots \rho_b]$ and $\mathbf{H}_0$ =unit matrix, diverges, one has to employ approximate solution and iteration matrix of lower bulk density as input for case of higher bulk density, at the same time, lower the value of relaxation factor α, for example $\alpha = 0.75$, the total iteration times are not beyond 30. For the traditional Broyles' mixing procedure, the iteration number needed to arrive at the true solution with $\varepsilon = 10^{-9}$ usually is high up to 500 for case of low $\rho_b\sigma^3$, for example $\rho_b\sigma^3 \leq 0.42$ with the initial value of $\mathbf{x}^{0^T} = [\rho_b, \rho_b, \ldots \rho_b]$. While for case of higher $\rho_b\sigma^3$, the iteration process also has to begin with the output of lower density case as input, the needed iteration number is high upto 1000 or 2000 or more. What is more, for case of higher $\rho_b\sigma^3$, the true solution with $\varepsilon = 10^{-9}$ will be never arrived at, only approximate solution with $\varepsilon = 10^{-3}$ can be found.

References

[1] D. Henderson. *Fundamentals of Inhomogeneous Fluids*, Marcel Dekker, New York (1992).

[2] Y. Burak, H. Orland. Manning condensation in two dimensions. *Phys. Rev. E*, **73**, 010501(R) (2006).

[3] L. Li, D. Bedrov, G.D. Smith. Water-induced interactions between carbon nanoparticles. *J. Phys. Chem. B*, **110**, 10509 (2006).

[4] Z. Su, M. Maroncelli. Simulations of solvation free energies and solubilities in supercritical solvents. *J. Chem. Phys.*, **124**, 164506 (2006).

[5] S. Zhou. Formalism for calculation of polymer-solvent-mediated potential. *Phys. Rev. E*, **74**, 011402 (2006).

[6] S. Zhou, A. Jamnik. Global and critical test of the perturbation density-functional theory based on extensive simulation of Lennard-Jones fluid near an interface and in confined systems. *J. Chem. Phys.*, **123**, 124708 (2005).

[7] S. Varga, D. Boda, D. Henderson, S. Sokolowski. Density functional theory and the capillary evaporation of a liquid in a slit. *J. Colloid and Interface Sci.*, **227**, 223 (2000).

[8] Z. Tang, L.E. Scriven, H.T. Davis. Density-functional perturbation theory of inhomogeneous simple fluids. *J. Chem. Phys.*, **95**, 2659 (1991).

[9] S. Zhou. Partitioned density functional approach for Lennard-Jones fluid. *Phys. Rev. E*, **68**, 061201 (2003).

[10] Y. Tang, J. Wu. Modeling inhomogeneous van der Waals fluids using an analytical direct correlation function. *Phys. Rev. E*, **70**, 011201 (2004).

[11] X.C. Zeng, Dw. Oxtoby. Applications of modified weighted density functional theory: freezing of simple liquids. *J. Chem. Phys.*, **93**, 2692 (1990).

[12] S. Zhou. Formally exact truncated nonuniform excess Helmholtz free energy density functional: test and application. *J. Phys. Chem. B*, **108**, 3017 (2004).

[13] S. Zhou. Reformulation of density functional theory for generation of the nonuniform density distribution. *Phys. Rev. E*, **63**, 061206 (2001).

[14] G.A. Martynov. *Fundamental Theory of Liquids. Method of Distribution Functions*, Adam Hilger, Bristol (1992).

[15] L. Verlet. Integral-equations for classical fluids .1. The hard-sphere case. *Mol. Phys.*, **41**, 183 (1980).

[16] D-M. Duh, A.D.J. Haymet. Integral equation theory for uncharged liquids: the Lennard-Jones fluid and the bridge function. *J. Chem. Phys.*, **103**, 2625 (1995).

[17] F. Ancilotto, F. Toigo. First-order wetting transitions of neon on solid CO2 from density functional calculations. *J. Chem. Phys.*, **112**, 4768 (2000).

[18] C. Balabanic, B. Borstnik, R. Milcic, A. Rubcic, F. Sokolic. Static and dynamic properties of liquids. In *Springer Proceedings in Physics*, M. Davidovic, A.K. Soper (Eds.), Vol. 40, p. 70, Springer, Berlin (1989).

[19] J.K. Johnson, J.A. Zollweg, K.E. Gubbins. The Lennard-Jones equation of state revisited. *Mol. Phys.*, **78**, 591 (1993).

[20] L. Verlet, J.-J. Weis. Equilibrium theory of simple liquids. *Phys. Rev. A*, **5**, 939 (1972).

[21] Y. Rosenfeld. Free-energy model for the inhomogeneous hard-sphere fluid mixture and density-functional theory of freezing. *Phys. Rev. Lett.*, **63**, 980 (1989).

[22] S. Zhou. Isostructural solid–solid transitions in binary asymmetrical hard sphere system: based on solvent-mediated potential. *J. Colloid and Interface Sci.*, **288**, 308 (2005).

[23] J.M. Ortega, W.C. Rheinboldt, Chapter 7. *Iterative Solution of Nonlinear Equations in Several Variables*, Academic Press. (1970).

[24] A.A. Broyles. Radial distribution functions from the Born-Green integral equation. *J. Chem. Phys.*, **33**, 456 (1960).

[25] S. Labik, A. Malijevsky, P. Vonka. A rapidly convergent method of solving the OZ equation. *Mole. Phys.*, **56**, 709 (1985).

[26] M.S. Wertheim. Exact solution of the Percus-Yevick integral equation for hard spheres. *Phys. Rev. Lett.*, **10**, 321 (1963).

[27] W.H. Press, B.P. Flannery, S.A. Teukolsky, W.T. Vetterling. *Numerical Recipes*, Cambridge University, New York (1986).

[28] C. Broyden. A new method of solving nonlinear simultaneous equations. *Comput. J.*, **12**, 95 (1969).